Journal of Sound and Vibration (2001) **245**(3), 433–455
doi:10.1006/jsvi.2001.3592, available online at http://www.idealibrary.com on IDEAL®

PREDICTING THE ACOUSTICAL RADIATION OF FINITE SIZE MULTI-LAYERED STRUCTURES BY APPLYING SPATIAL WINDOWING ON INFINITE STRUCTURES

M. Villot, C. Guigou and L. Gagliardini†

C.S.T.B. Noise and Vibration Department, 24, *Rue Joseph Fourier*, 38400 *Saint-Martin-d'Hères*, *France*

(*Received* 19 *April* 2000, *and in final form* 10 *November* 2000)

A new technique based on a spatial windowing of plane waves is presented in order to take into account the finite size of a plane structure in sound radiation and sound transmission calculation. This technique leads to predicted results which are much closer to experimental measurements than the classical wave approach applied to an infinite structure. In the first part, the principle of the technique is described as well as the derivation of the modified sound radiation efficiency. In the second part, some predicted results, including the sound transmission index of an aluminium plate, a double glazing panel and a multi-layer panel, and the radiation efficiency of a mechanically excited metal plate, are presented and compared to experimental results in order to validate the spatial windowing technique. The effect of the structure size on both sound transmission (acoustical excitation) and sound radiation (mechanical excitation) is also discussed.

1. INTRODUCTION

The wave approach is generally used to study the sound transmission through planar structures at high frequencies; it consists of calculating the sound reduction index of an infinite plane structure excited by a single or random (diffuse field) incident plane wave. This approach has the advantage of clearly showing the dominant physical phenomena involved, such as the critical frequency for single leaf partitions or the resonance frequency for double leaf partitions (see for example, Chapter 4 in reference [1]); it greatly simplifies the calculation of sound transmission through multi-layered structures by means of the transfer matrix technique as developed by Munjal [2] and always corresponds to relatively short computation time. However, the calculated results are often quite different from these experimental curves: for example, the calculated sound reduction index associated with a single leaf panel generally shows important discrepancies especially at low frequencies. Until now, the most frequently used "trick" to reduce differences between experimental results and the wave approach, has been to limit the maximum incidence angle (i.e., the diffuseness) of the acoustic field incident on the infinite structure [3–5]. This of course strongly influences the results (as will be seen in section 3); however, the general behavior is not much improved at low frequencies and the slope of the transmission index remains unchanged.

†Currently working at P.S.A. Peugeot-Citroën, 18 Rue des Fauvelles, B. P. 16, 92256 La Garenne-Colombes Cedex, France.

0022-460X/01/330433 + 23 $35.00/0

The wave approach also gives poor results compared to experimental ones when calculating the sound radiated by a mechanically excited planar structure; any free plane wave travelling on the infinite structure does not radiate any power below the critical frequency, while the same wave, combined to form a flexural mode does radiate power (see section 2.5 in reference [1]).

As clearly stated in reference [1], the two main factors that cause the sound performance of a real bounded panel in a rigid baffle to differ significantly from the theoretical performance of an unbounded panel are (i) the existence of structural modes and associated resonance frequencies and (ii) the diffraction by the aperture in the baffle that contains the panel. An additional difference between calculated and measured results comes from the influence of room boundaries on transmission through partitions that separate two rooms.

Some authors have developed expressions for the radiation efficiency of panels including the diffraction effect; using the wave approach to determine the transmission loss through a finite size single wall at low frequency (mass driven response), Sato [6] and Rindell [7] developed an integral expression of the radiation efficiency in the special case of a rectangular panel in a baffle forced by a plane sound wave at oblique incidence. In order to obtain the transmission index for random incidence excitation, Rindell [7] used a mean radiation efficiency ("diffuse" radiation efficiency) applied to the mass driven approximation of the transmission loss. Ljunggren [8] also used the same approach to obtain the radiation efficiency of a one-dimensional structure. On the other hand, several authors have developed expressions for the radiation efficiency of finite size panels using the modal approach; among them, Sewel [9] and more recently Leppington [10, 11] have now given classical and well-validated results. The technique presented in this paper is based on the wave approach, and therefore takes advantage of the relative simplicity of the transfer matrix approach for infinite multi-layered structures (without any modal consideration) but also includes the diffraction effect on sound radiation and sound transmission associated with the finite size of a structure. The technique is based on a windowing technique, close to the technique used in references [6–8] but presented in a more general format. Both the determination of the transmission loss for random incidence and the determination of the sound radiation from a mechanical point driven structure are considered.

In section 1 of the paper, the principle of the technique is given as well as the derivation of the modified radiation efficiencies, transmission loss and radiated power for both acoustical and mechanical excitations; the technique is compared to the other existing, similar but less general methods mentioned before [6–8]. In section 2, some calculated results including the sound reduction index of an aluminium plate, double glazing and a multi-layer panel as well as the radiation efficiency and the power radiated from a mechanically excited metal plate are given and compared to experimental results in order to validate the spatial windowing technique and to show the improvements obtained, compared to the classical wave approach. The effect of the aperture size on both sound transmission and sound radiation (case of mechanical excitation) is also briefly discussed.

2. THE SPATIAL WINDOWING TECHNIQUE

2.1. PRINCIPLE

The principle of the technique consists of spatially windowing the excitation pressure field (case of acoustical excitation), calculating the resulting vibration velocity field of the infinite structure and spatially windowing this vibration field before calculating the radiated field. In the case of mechanical excitation, only the spatial windowing of the vibration velocity field of the infinite structure is performed before calculating the radiated field.

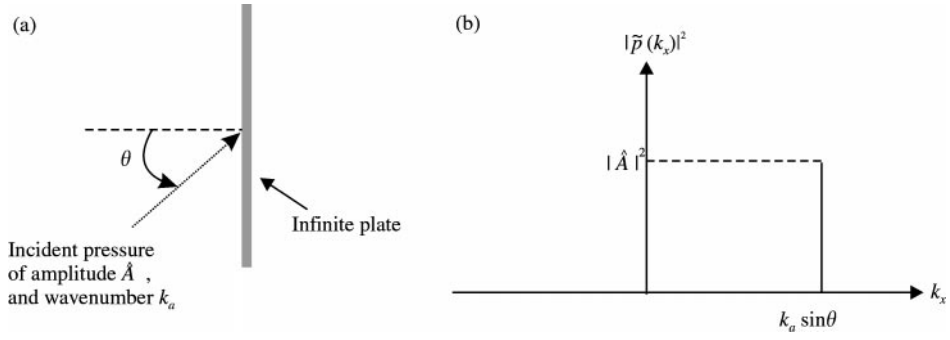

Figure 1. (a) Acoustically excited infinite plate and (b) associated incident pressure wavenumber spectrum.

In this section, a qualitative explanation of the spatial windowing technique is given in the wavenumber domain for a one-dimensional structure in order to better understand the derivation of section 2.2.

2.1.1. *Acoustical excitation*

Figure 1(a) shows an infinite plate acoustically excited by an oblique (angle θ) incident plane wave of amplitude A. In the wavenumber domain and at a given frequency ω, the excitation pressure field is then represented by a delta Dirac function as depicted in Figure 1(b). A single wavenumber $k_x = k_a \sin\theta$ is represented in the excitation spectrum and a single wave with the particular wavenumber $k_p = k_a \sin\theta$ will propagate in the infinite structure. Note that k_a represents the wavenumber in the surrounding fluid (air) and k_p the structural wavenumber propagating in the structure (also denoted as trace wavenumber [1]).

In the case of a finite size system, it can be considered that the incident pressure wave goes through a diaphragm (of length a) before impinging on the infinite structure as shown in Figure 2(a). In that case, the incident pressure field wavenumber spectrum, as seen in Figure 2(b), is spread over the entire wavenumber domain. It should be noticed that even if the excitation frequency is smaller than the plate critical frequency (i.e., the free flexural wavenumber k_f is greater than the acoustical wavenumber k_a), the windowed pressure field will not only generate a forced travelling wave (k_x close to $k_p = k_a \sin\theta$) but also a free travelling flexural wave (k_x close to k_f) since there is excitation energy around k_f.

2.1.2. *Structural excitation*

A structural excitation distributed over the small length l of the structure, as shown in Figure 3(a) is now considered. This type of mechanical load can be decomposed into an infinite number of travelling normal stress waves as shown in Figure 3(b). In this case, no windowing is required at the excitation stage.

2.1.3. *Radiation*

Figure 4(a) shows a given flexural plane wave (wavenumber k_p) travelling along an infinite structure in the spatial domain (real space). The velocity wavenumber spectrum includes, in that case, a single component at $k_x = k_p$ as presented in Figure 4(b). Only wavenumbers smaller than the wavenumber in the surrounding fluid k_a ($k_x < k_a$), i.e.,

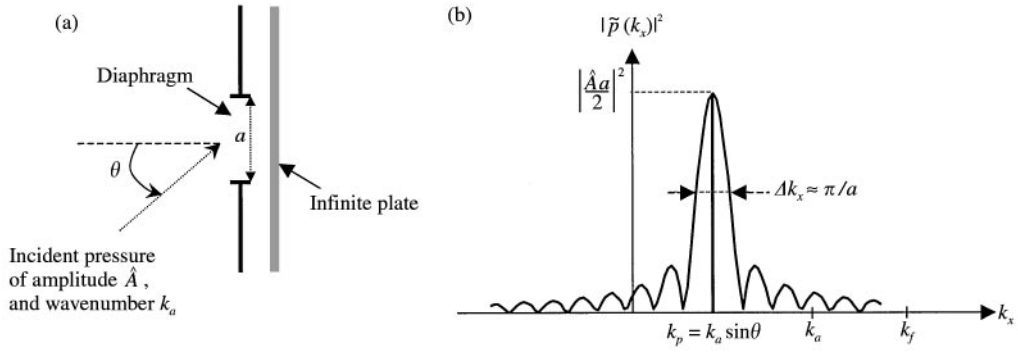

Figure 2. (a) Spatial windowing of acoustic incident field exciting an infinite plate and (b) associated incident pressure wavenumber spectrum.

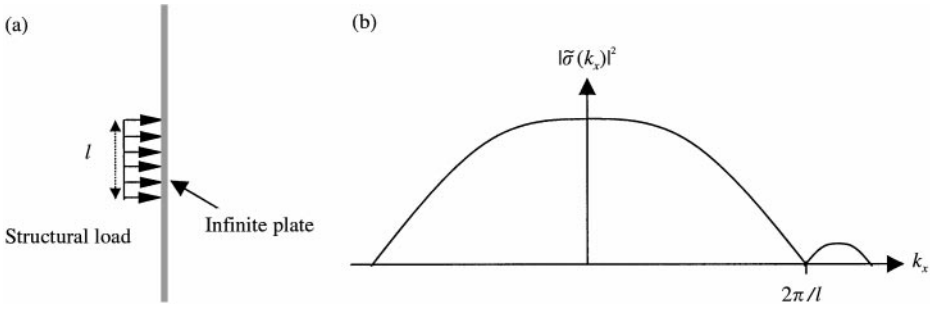

Figure 3. (a) Structural excitation on an infinite plate and (b) associated stress wavenumber spectrum.

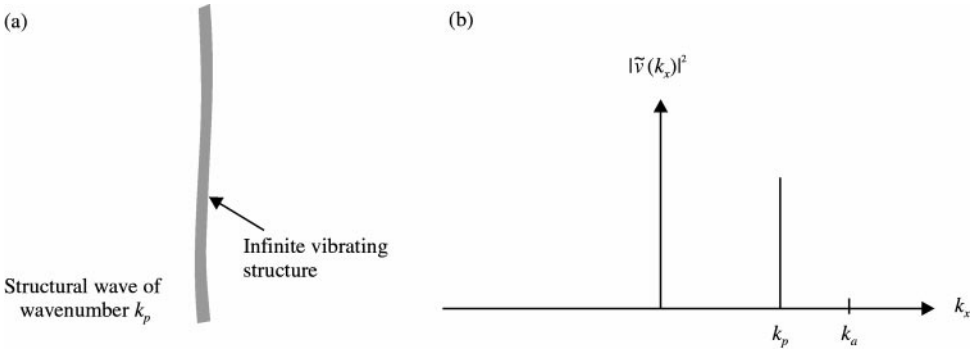

Figure 4. (a) Structural wave propagating in an infinite structure and (b) associated velocity wavenumber spectrum.

corresponding to a supersonic wave, participate in sound radiation; therefore, in the case presented in Figure 4(b), sound radiation will occur (since $k_p < k_a$). On the other hand, if $k_p > k_a$, no sound will be radiated in the far-field.

Considering only the length of the structure that contributes to the sound radiation (see Figure 5(a)), leads to the velocity wavenumber spectrum shown in Figure 5(b). The energy is once again spread over the whole wavenumber domain. In this case, if the

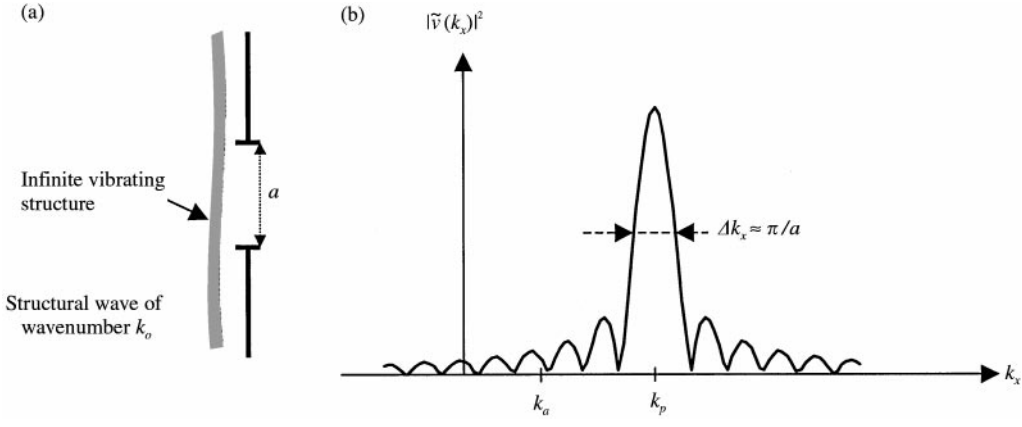

Figure 5. (a) Spatial windowing of a structural wave propagating in an infinite structure and (b) associated velocity wavenumber specturm.

structural wavenumber k_p is larger than k_a (as shown in Figure 5(b)), wavenumber components associated with sound radiation (i.e., $k_x < k_a$) are present in the velocity wavenumber spectrum, and the radiation efficiency will be small but not zero.

2.2. RADIATION EFFICIENCY ASSOCIATED WITH SPATIAL WINDOWING

A structural wave of wavenumber k_p is now assumed to propagate on an infinite two-dimensional structure in the direction ψ; the wavenumber components k_{px}, k_{py} can be written as

$$k_{px} = k_p \cos\psi,$$

$$k_{py} = k_p \sin\psi. \tag{1}$$

The time dependence of the different fields is assumed to be in the form $e^{i\omega t}$ and will be omitted for conciseness. The velocity field in the spatial domain can then be written as

$$v(x, y) = \hat{v}\, e^{-ik_{px}x} e^{-ik_{py}y} \tag{2}$$

Consider only that part of a surface of area S (of length L_x and width L_y) of the structure which contributes to the sound radiation; the velocity field in the wavenumber domain is then defined by taking the spatial Fourier transform

$$\tilde{v}(k_x, k_y) = \hat{v} \int_{-L_x/2}^{L_x/2} \int_{-L_y/2}^{L_y/2} e^{-ik_{px}x}\, e^{-ik_{py}y}\, e^{ik_x x}\, e^{ik_y y}\, dx\, dy$$

$$= \hat{v}\, L_x L_y \frac{\sin((k_x - k_p\cos\psi)L_x/2)}{((k_x - k_p\cos\psi)L_x/2)} \cdot \frac{\sin((k_y - k_p\sin\psi)L_y/2)}{((k_y - k_p\sin\psi)L_y/2)}. \tag{3}$$

The radiated power calculated from the wavenumber spectrum of the velocity field can be expressed, using polar co-ordinates ($k_x = k_r\cos\phi$; $k_y = k_r\sin\phi$) by reference [1], as

$$\Pi(k_p, \psi) = \frac{\rho_a c_a}{8\pi^2} \int_0^{k_a} \int_0^{2\pi} \frac{|\tilde{v}(k_r\cos\phi, k_r\sin\phi)|^2}{\sqrt{k_a^2 - k_r^2}}\, k_a k_r\, d\phi\, dk_r, \tag{4}$$

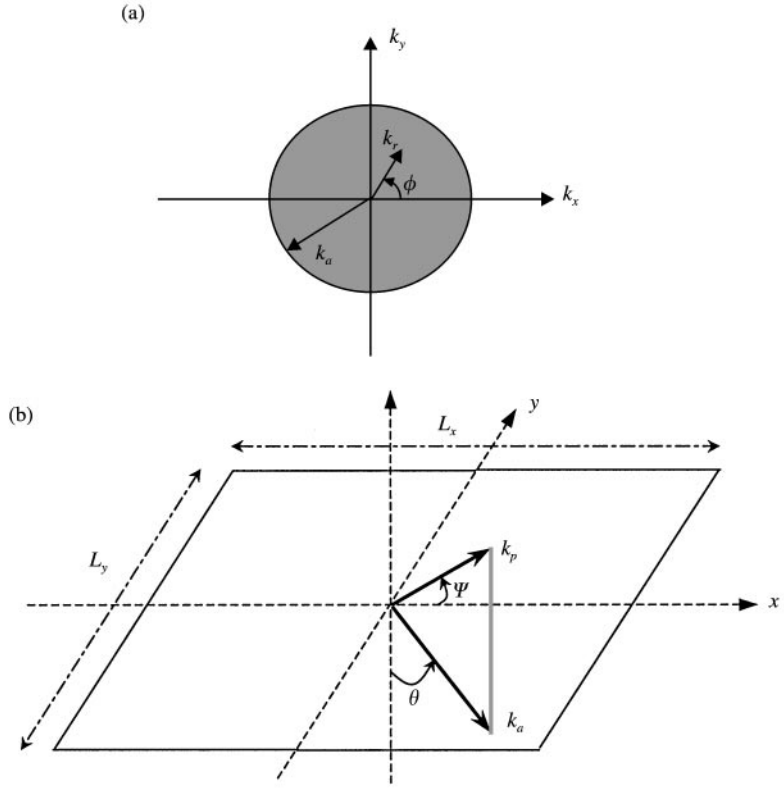

Figure 6. (a) Wavenumber components contributing to sound radiated power and (b) Schematic of a 3D acoustic plane wave excitation (incidence angle θ).

where k_a is the wavenumber in the air (see above) and ρ_a is the air density. It may be noted that the expression $\rho_a c_a \; k_a/\sqrt{k_a^2 - k_r^2}$ in equation (4) corresponds to the radiation impedance [1, 12]. As shown in Figure 6(a), only wavenumber components of the velocity inside the circle of radius k_a (often called radiation circle) participate in the sound radiated power.

The radiation efficiency can be calculated from

$$\sigma(k_p, \psi) = \frac{\Pi(k_p, \psi)}{\rho_a c_a S \langle v^2 \rangle}, \tag{5}$$

where $\langle v^2 \rangle$ is the mean-squared velocity defined as

$$\langle v^2 \rangle = \frac{1}{2S} \int_S |v(x, y)|^2 \, \mathrm{d}S = \frac{|\hat{v}|^2}{2}. \tag{6}$$

Using equations (3), (4) and (6) in equation (5) leads to the following expression of the radiation efficiency for a travelling structural wave

$$\sigma(k_p, \psi) = \frac{S}{\pi^2} \int_0^{k_a} \int_0^{2\pi} \frac{1 - \cos((k_r \cos\phi - k_p \cos\psi) L_x)}{[(k_r \cos\phi - k_p \cos\psi) L_x]^2} \cdot \frac{1 - \cos((k_r \sin\phi - k_p \sin\psi) L_y)}{[(k_r \sin\phi - k_p \sin\psi) L_y]^2} \times \frac{k_a k_r}{\sqrt{k_a^2 - k_r^2}} \, \mathrm{d}\phi \, \mathrm{d}k_r. \tag{7}$$

TABLE 1

Material characteristics

	Aluminum	Glass	Steel	Gypsum Board
Thickness	1·1 mm	4 mm	1 mm	15 mm
Young's Modulus	70·0 GN/m^2	62·0 GN/m^2	210. GN/m^2	2·5 GN/m^2
Density	2700 kg/m^3	2500 kg/m^3	7850 kg/m^3	690 kg/m^3
The Poisson ratio	0·33	0·22	0·3	0·1
Damping	1%	5%	3·5% for $f \leqslant 250$ Hz linear decrease to 1·5% for $f \geqslant 700$ Hz	5% for $f \leqslant 100$ Hz linear decrease to 2·5% for $f \geqslant 2500$ Hz

It has been found that the dependence of the radiation efficiency (equation (7)) on the angle ψ is slight. Therefore, in order to condense the results and present the variation of the radiation efficiency only as a function of frequency (in this section) or frequency and angle of incidence θ (in the next section), the radiation efficiency is averaged over ψ. However, for the calculation of the transmission loss as presented below in section 2.3.2 as well as for the calculation of the radiated power in the case of mechanical excitation as presented in section 2.4.1, the radiation efficiency given by equation (7) (i.e., not averaged) is used.

The structural averaged radiation efficiency $\langle\sigma(k_p)\rangle_\psi$ is obtained as the triple integral

$$\langle\sigma(k_p)\rangle_\psi = \frac{S}{2\pi^3}\int_0^{2\pi}\int_0^{k_a}\int_0^{2\pi}\frac{1-\cos((k_r\cos\phi - k_p\cos\psi)L_x)}{[(k_r\cos\phi - k_p\cos\psi)L_x]^2}\cdot\frac{1-\cos((k_r\sin\phi - k_p\cos\psi)L_y)}{[(k_r\sin\phi - k_p\cos\psi)L_y]^2}$$

$$\times\frac{k_a k_r}{\sqrt{k_a^2 - k_r^2}}\,\mathrm{d}\phi\,\mathrm{d}k_r\,\mathrm{d}\psi. \tag{8}$$

The frequency spectrum of $\langle\sigma(k_p)\rangle_\psi$ depends on the dispersion curve $k_p(\omega)$ of the plate considered; here, the example of the bending wavenumber k_p of a thin plate (proportional to $\sqrt{\omega}$) is chosen. The surface S of the radiating part of the plate is of length $L_x = 1{\cdot}4$ m and width $L_y = 1{\cdot}1$ m. The plate material properties (gypsum board) are given in Table 1 except for the damping factor which is taken to be zero in this case. Figure 7 presents the radiation efficiency obtained using equation (8). It can be seen that, below the critical frequency of the plate (marked f_c in Figure 7), the radiation efficiency obtained with the spatial windowing technique is small but not null; as stated in the introduction, the radiation efficiency for an infinite structure on which a propagating bending wave travels would be zero below the critical frequency. As expected, the radiation efficiency tends to unity for frequencies higher than the critical frequency.

2.3. APPLYING SPATIAL WINDOWING TO SOUND TRANSMISSION

2.3.1. *Radiation efficiency*

For an incident acoustic plane wave, the wavenumber k_p is related to the incident angle θ by $k_p = k_a \sin\theta$ as shown in Figure 6(b). In this case, the radiation efficiency for an infinite system (no spatial windowing) is given by

$$\sigma_{inf} = 1/\cos\theta. \tag{9}$$

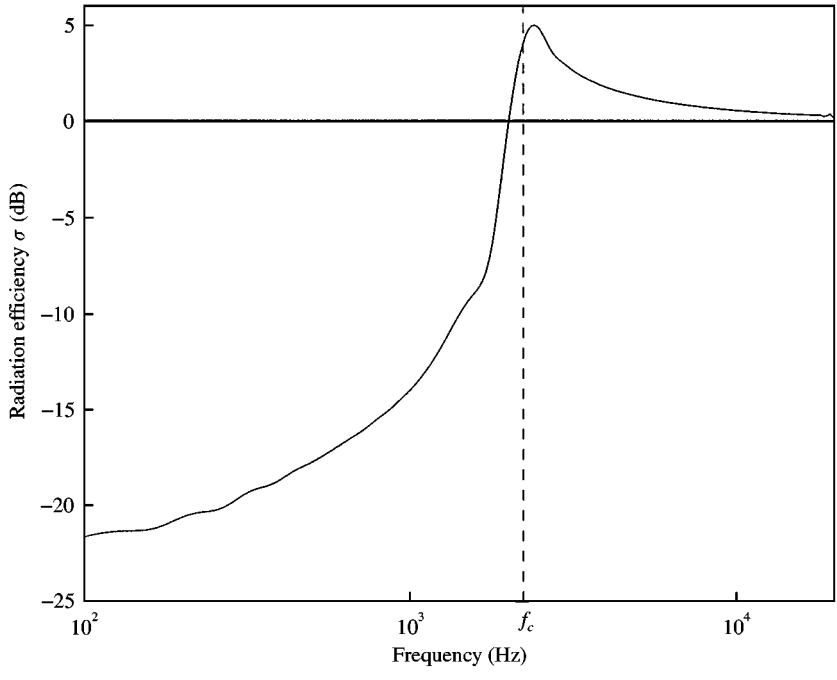

Figure 7. Radiation efficiency $\langle \sigma(k_p) \rangle_\psi$ after spatial windowing for a plate in bending.

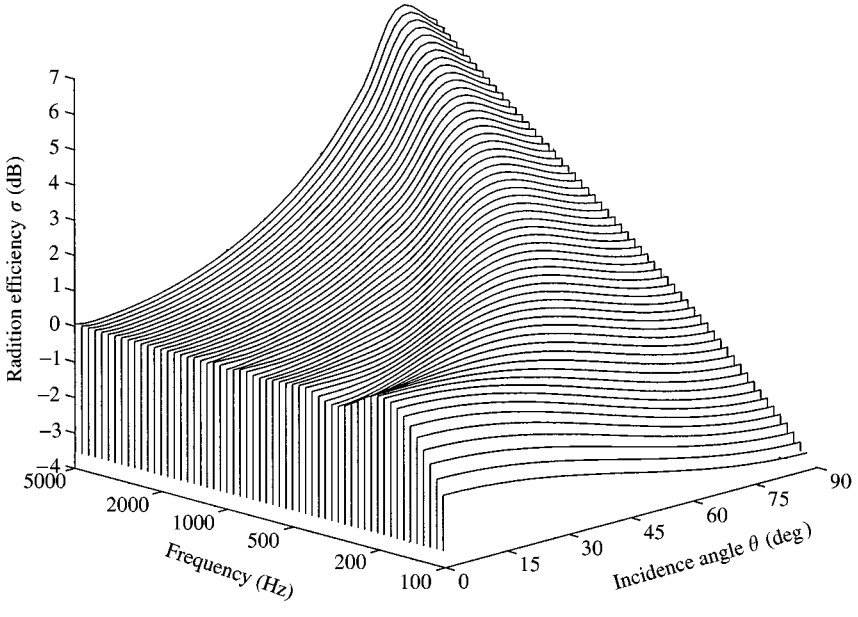

Figure 8. Radiation efficiency of an infinite structure after applying the spatial windowing technique.

Figure 8 shows the diffuse field radiation efficiency $\langle \sigma(k_a \sin \theta) \rangle_\psi$ associated with the spatial filtering of the infinite structure (equation (8)) for an acoustic wave excitation as a function of frequency and incidence angle. It is important to note that $\langle \sigma(k_a \sin \theta) \rangle_\psi$ does not depend on the structure considered but only on the size of the rectangular aperture chosen. In this

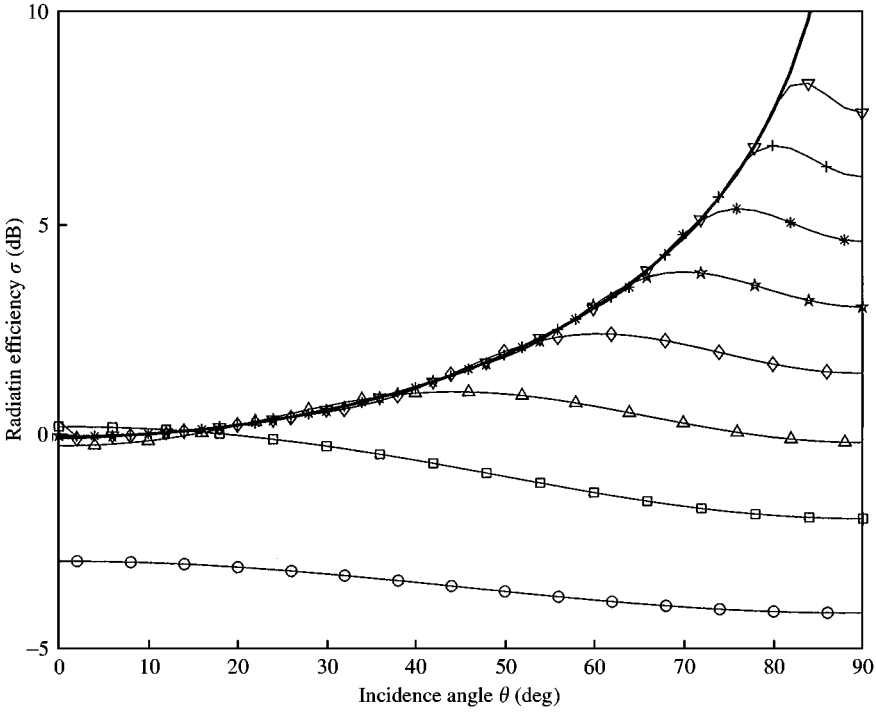

Figure 9. Radiation efficiency of an infinite structure before and after applying the spatial windowing technique; — infinite structure, ○ spatially windowed structure $k_aL = 2$, □ spatially windowed structure $k_aL = 4$, △ spatially windowed structure $k_aL = 8$, ◇ spatially windowed structure $k_aL = 16$, ☆ spatially windowed structure $k_aL = 32$, ∗ spatially windowed structure $k_aL = 64$, + spatially windowed structure $k_aL = 128$, ▽ spatially windowed structure $k_aL = 256$.

example, the surface S of the structure contributing to the sound radiation is of length $L_x = 1{\cdot}4$ m and width $L_y = 1{\cdot}1$ m. Figure 9 shows the radiation efficiency for different values of the non-dimensional parameter k_aL (where L is the characteristic dimension defined as $\sqrt{L_xL_y}$) of the spatially windowed system as well as that of the infinite system (equation (9)). Figure 9 is similar to that presented in references [6, 7] in the case of a square panel. For the infinite system, the radiation efficiency approaches infinity as the angle of incidence θ tends to 90°. In the case of the spatially windowed system, the radiation efficiency remains finite even for $\theta = 90°$. Two main regions can be observed in Figures 8 and 9:

1. For $k_aL < 4$, (i.e., for frequencies below about 175 Hz for the spatial window considered), the radiation efficiency of the finite structure (using spatial filtering) is lower than that of the infinite system for any angle of incidence and does not significantly vary with the angle of incidence θ.

2. For $k_aL > 4$, the radiation efficiency of the finite structure (using spatial filtering) increases with the angle of incidence θ, following the radiation efficiency of the infinite system, up to a certain incidence angle and does not significantly vary afterwards, remaining finite for $\theta = 90°$.

Therefore at low frequency, the radiation from the finite structure will always be less than that of the associated infinite structure.

2.3.2. *Sound transmission*

The spatial windowing is now directly applied to the problem of sound transmission through a structure. The sound reduction index associated with the infinite structure is

assumed to be known. Note that in the case of a multi-layered structure, it can be calculated using the transfer matrix method as described in references [2, 5]. The sound reduction index for the infinite structure is denoted by $\tau_{inf}(\theta)$, where θ is the incidence angle of the plane wave excitation of amplitude $\hat{p}_i$, and is expressed as the ratio of the transmitted sound intensity to the incident intensity, i.e.

$$\tau_{inf}(\theta) = \frac{I_{inf\_trans}}{I_{inf\_inc}} = \frac{\rho_a c_a}{2} \frac{|\hat{v}|^2}{\cos\theta} \frac{1}{I_{inf\_inc}}, \tag{10}$$

where $\rho_a c_a/\cos\theta$ represents the wave radiation impedance. Note that $\hat{v}$ represents the normal particle velocity at the interface of the outer layer with the fluid of the receiving half space. It coincides with the structure normal velocity if the outer layer is solid; in the case of a porous outer layer, it is given by a combination of the solid phase and fluid phase normal velocity of the porous material (see references [5, 13] for example).

Applying first the spatial windowing to the radiation process, a new sound transmission index can be defined by

$$\tau_{1\_finite}(\theta, \psi) = \frac{\Pi_{finite\_trans}(k_a \sin\theta, \psi)}{I_{inf\_inc} S} \tag{11}$$

with $\Pi_{finite\_trans}(k_a \sin\theta, \psi)$ the transmitted power given by equation (4), where the velocity field of the infinite structure has been spatially windowed. Using the derivations presented in section 2.2, equation (11) can be rewritten as

$$\tau_{1\_finite}(\theta, \psi) = \frac{I_{inf\_trans}}{I_{inf\_inc}} \frac{\Pi_{finite\_trans}(k_a \sin\theta, \psi)}{I_{inf\_trans} S} = \tau_{inf}(\theta) \frac{\Pi_{finite\_trans}(k_a \sin\theta, \psi)}{S\, \rho_a c_a/2\ \ |\hat{v}|^2/\cos\theta}$$

$$= \tau_{inf}(\theta)\, \sigma(k_a \sin\theta, \psi) \cos\theta, \tag{12}$$

where equations (5) and (6) have been used to express $\Pi_{finite\_trans}(k_a \sin\theta, \psi)$.

The same process can be applied to obtain the effect of spatially windowing the incident pressure field $p_i(x, y) = \hat{p}_i\, e^{-ik_a \sin\theta \cos\psi . x}\, e^{-ik_a \sin\theta \sin\psi . y}$; a correcting factor $\tau_{2\_finite}(\theta, \psi)$ can be defined as

$$\tau_{finite}(\theta, \psi) = \tau_{2\_finite}(\theta, \psi)\ \tau_{1\_finite}(\theta, \psi) \tag{13}$$

with $\tau_{finite}(\theta, \psi)$ the transmission factor resulting from windowing both the excitation pressure field and the radiated field. The correcting factor $\tau_{2\_finite}(\theta, \psi)$ can be expressed as

$$\tau_{2\_finite}(\theta, \psi) = \frac{\Pi_{finite\_inc}(k_a \sin\theta, \psi)}{I_{inf\_inc} S} = \frac{\Pi_{finite\_inc}(k_a \sin\theta, \psi)}{S|\hat{p}_i|^2 \cos\theta/2\rho_a c_a}. \tag{14}$$

The particle velocity component normal to the x, y plane of the incident field before spatially windowing can be expressed in the real space as

$$v_{i,n}(x, y) = p_i(x, y).\cos\theta/\rho_a c_a. \tag{15}$$

The incident power $\Pi_{finite\_inc}(k_a \sin\theta, \psi)$ can then be obtained from this normal particle velocity in exactly the same way as the power $\Pi(k_p, \psi)$ radiated by the windowed structure was obtained in section 2.2 from the flexural velocity of the structure; equations (5) and (6)

can be used and $\Pi_{finite\_inc}(k_a \sin\theta, \psi)$ can be expressed as

$$\Pi_{finite\_inc}(k_a \sin\theta, \psi) = \rho_a c_a S.\sigma(k_a \sin\theta, \psi).\frac{|\hat{v}_{i,n}|^2}{2} = (|\hat{p}_i|^2 \cos^2\theta/2\rho_a c_a)\, S.\sigma(k_a \sin\theta, \psi) \quad (16)$$

and equation (14) becomes

$$\tau_{2\_finite}(\theta, \psi) = \cos\theta\, \sigma(k_a \sin\theta, \psi). \quad (17)$$

The transmission index associated with the finite structure after applying the spatial windowing technique is then given by

$$\tau_{finite}(\theta, \psi) = \tau_{2\_finite}(\theta, \psi)\, \tau_{1\_finite}(\theta, \psi) = \tau_{inf}(\theta, \psi)\, [\sigma(k_a \sin\theta, \psi) \cos\theta]^2. \quad (18)$$

Therefore, for an acoustic excitation field, the infinite system is affected twice by the modification of the radiation efficiency (as explained in section 2); both the incident field and the radiation are modified and the modification is applied to the incidence-dependent transmission index. Note that $\sigma(k_a \sin\theta, \psi)$ does not depend on the structure considered but only on the size of the rectangular window; the radiation efficiencies corresponding to typical dimensions of walls, glazing, etc. can therefore be pre-calculated.

The transmission index for a diffuse field excitation is finally expressed by

$$\tau_{diffuse} = \frac{\int_0^{\theta_{lim}} \int_0^{2\pi} \tau(\theta, \psi) \sin\theta \cos\theta \, \mathrm{d}\theta \, \mathrm{d}\psi}{\int_0^{\theta_{lim}} \int_0^{2\pi} \sin\theta \cos\theta \, \mathrm{d}\theta \, \mathrm{d}\psi}, \quad (19)$$

where θ_{lim} is the limiting angle defining the diffuseness of the incident field, equal to $\pi/2$ (i.e., 90°) in the results presented in this paper. Note that θ_{lim} was between 70° and 85° (instead of 90°) in references [3–5] in order to reduce the differences between theory (infinite system) and experiments. Equation (19) is valid for $\tau(\theta, \psi)$ taken to be either $\tau_{inf}(\theta)$ (in this case, the sound reduction index is dependent of incidence angle ψ and the integration with respect to ψ is then straightforward) or $\tau_{finite}(\theta, \psi)$ given by equation (18).

As previously mentioned, equations (18) and (19) can be applied to any multi-layered structure, as long as the incidence-dependant sound transmission index $\tau_{inf}(\theta)$ is known; the type of different layers is of no importance for the method presented here as long as the normal particle velocity with the surrounding space on both the incident and the receiving side is correctly evaluated (using the appropriate interface conditions).

2.4. APPLYING SPATIAL WINDOWING TO SOUND RADIATION FROM STRUCTURALLY EXCITED STRUCTURE

The structure is now assumed to be subjected to a structural excitation (force). Therefore, an infinite number of propagating waves, generated by an infinite number of travelling normal stress waves as explained in section 2.1.2, propagate in the structure. The velocity field $\tilde{v}_{inf}(k_x, k_y)$ in the wavenumber domain for the infinite structure is assumed to be known. In the case of a multi-layered structure, it is calculated using the transfer matrix method (at one of the two free surfaces of the multi-layered structure considered).

According to the derivations given in section 2.2, the power radiated by the windowed structure and associated to the velocity component $\tilde{v}_{inf}(k_p \cos\psi, k_p \sin\psi)$ (i.e., to the structural wave of wavenumber k_p) can be expressed using equations (5) and (6) as

$$\Pi_{wave\_rad}(k_p, \psi) = \rho_a c_a\, \sigma(k_p, \psi)\, S\langle v^2\rangle_{infinite} \quad (20)$$

where, in this case

$$\langle v^2 \rangle_{infinite} = \frac{1}{2} |v_{inf}(k_p \cos\psi,\, k_p \sin\psi|^2. \tag{21}$$

Note that the radiated power modified by the spatial windowing is an incidence dependent quantity. For a given frequency, the power radiated by the windowed structure can then be calculated in the wavenumber domain according to Parseval's theorem as

$$\Pi_{finite\_rad}(\omega) = \frac{1}{2\pi} \int_{k_p=0}^{\infty} \int_{\psi=0}^{\infty} \Pi_{wave\_rad}(k_p, \psi)\, \mathrm{d}k_p\, \mathrm{d}\psi. \tag{22}$$

Once again, this derivation is valid if the outer layer on the radiating side is made of porous material; the velocity used in equation (21) is then the normal particle velocity at the radiating interface.

Note that the radiated power given by equation (22) does not take into account the entire vibrational energy stored in the infinite plate but only the energy stored inside the window; in order to have a proper energy balance in between the power injected by the point force, vibrational energy stored in the plate and the radiated power, a radiation efficiency $\sigma_{finite}(\omega)$ must be calculated, the correct power radiated being expressed as

$$\Pi_{rad}(\omega) = \sigma_{finite}(\omega)\, \rho_a c_a S \langle v^2 \rangle_{infinite}, \tag{23}$$

where the product $S\langle v^2 \rangle_{infinite}$ represents the entire vibrational energy stored in the infinite structure which can be written according to Parseval's theorem as

$$S\langle v^2 \rangle_{infinite} = \frac{1}{4\pi^2} \frac{1}{2} \int_{-\infty}^{+\infty} \int_{-\infty}^{+\infty} |\tilde{v}_{inf}(k_x, k_y)|^2\, \mathrm{d}k_x\, \mathrm{d}k_y. \tag{24}$$

The radiation efficiency $\sigma_{finite}(\omega)$ is defined as

$$\sigma_{finite}(\omega) = \frac{\Pi_{finite\_rad}(\omega)}{\rho_a c_a S \langle v^2 \rangle_{finite}}. \tag{25}$$

The mean-squared velocity associated with the spatially windowed structure $\langle v^2 \rangle_{finite}$ can be obtained either from the velocity field in the wavenumber domain of the spatially windowed structure $\tilde{v}_{finite}(k_x, k_y)$ using Parseval's theorem or from the velocity field in the spatial domain of the infinite structure $v_{infinite}(x, y)$

$$\langle v^2 \rangle_{finite} = \begin{cases} \dfrac{1}{4\pi^2} \dfrac{1}{2S} \displaystyle\int_{-\infty}^{+\infty} \int_{-\infty}^{+\infty} |\tilde{v}_{finite}(k_x, k_y)|^2\, \mathrm{d}k_x\, \mathrm{d}k_y \\ \text{or} \\ \dfrac{1}{2S} \displaystyle\int_S |v_{infinite}(x, y)|^2\, \mathrm{d}S. \end{cases} \tag{26}$$

The velocity field in the wavenumber domain of the spatially windowed structure $\tilde{v}_{finite}(k_x, k_y)$ can be expressed as a convolution product, i.e.,

$$\tilde{v}_{finite}(k_x, k_y) = \tilde{v}_{inf}(k_x, k_y) \otimes \left[L_x L_y \frac{\sin(k_x L_x/2)}{(k_x L_x)/2} \cdot \frac{\sin(k_y L_y/2)}{(k_y L_y)/2} \right], \tag{27}$$

where $\otimes$ denotes the convolution product.

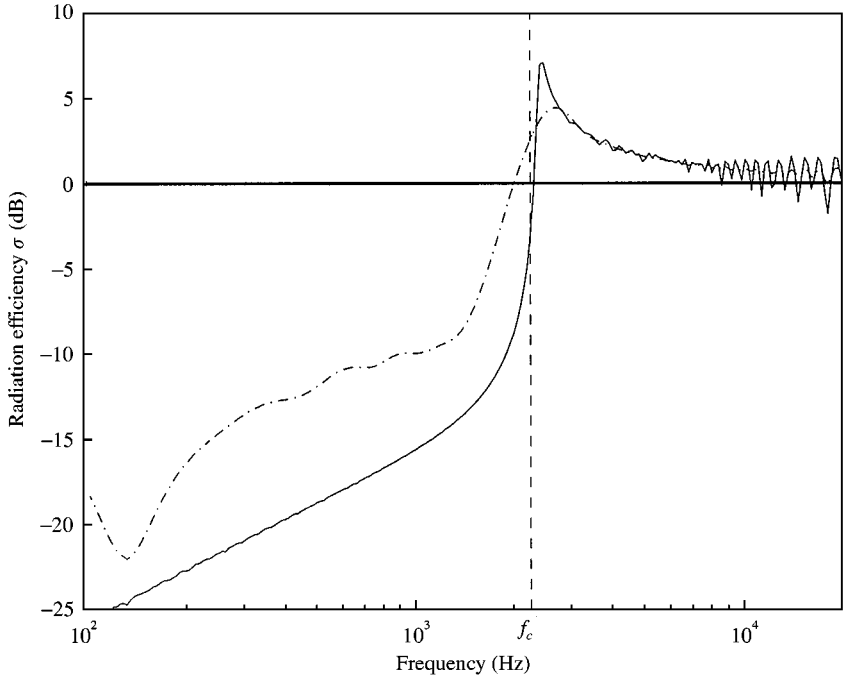

Figure 10. Radiation efficiency of an infinite structure excited by a point force, before and after applying the spatial windowing technique; — infinite system, —·— spatially windowed system.

The velocity field in the spatial domain of the infinite structure $v_{infinite}(x, y)$ can be obtained using the inverse Fourier transform of the velocity field in the wavenumber domain of the infinite structure $\tilde{v}_{infinite}(k_x, k_y)$. The convolution product or the inverse Fourier transform can be numerically calculated. The convolution product method is in general, in terms of time computation, more consuming than the inverse Fourier transform.

The radiation efficiency $\sigma_{finite}(\omega)$ can therefore be calculated using equations (25), (22) and (26) and the correct power radiated can finally be calculated using equations (23) and (24).

The same structure (gypsum board) with the same dimensions as in section 2.2 is now considered to illustrate the previous derivations. In the case of the spatially windowed structure, the excitation force is taken to be located at the center of the plate. The radiation efficiency for the infinite and spatially windowed structure is shown in Figure 10. This time, for the infinite system and at frequencies much lower than the critical frequency (marked f_c in Figure 10), the radiation efficiency is not null due to the fact that supersonic waves generated by supersonic stress waves exist (see section 2.1.2) and contribute to the sound radiation. By spatially windowing the system, the radiation efficiency is increased for frequencies much lower than the critical frequency, since more supersonic waves participate to the sound radiation as explained in section 2.1.3. The low frequency deep in the radiation efficiency (around 130 Hz) occurs when the free flexural wavelength ($\lambda_f = 2\pi/k_f$) is half of the system characteristic dimension ($L = \sqrt{L_x L_y}$). As expected, for frequencies close to and larger than the critical frequency, spatial windowing has little impact on the radiation efficiency.

Note that the position of the point force is also taken into account by the windowing technique. At the limit, the point force can be located out of the spatial window chosen, in

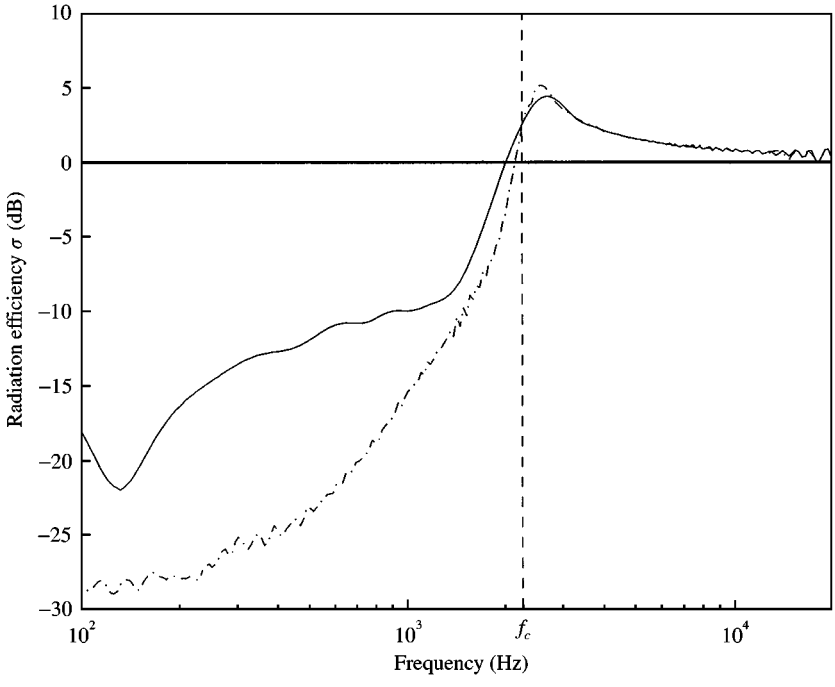

Figure 11. Radiation efficiency of a spatially windowed infinite structure excited by a point force—Force position effect; — spatially windowed system with forced centred, —·— spatially windowed system with forced out of spatial window.

order to cancel the near field effect. Figure 11 shows that, for a force located at 3·5 m in the x direction and 2·75 m in the y direction from the centre of the system (i.e., out of the spatial window considered), the radiation efficiency is, as expected, lower than the one with near field effect (point force in the middle of the window) for frequencies lower than the critical frequency. For frequencies close to and larger than the critical frequency, the radiation efficiency does not change significantly with force location.

3. EXPERIMENTAL VALIDATION

In this section, some results obtained using the wave approach with the spatial windowing technique are presented and compared to experimental results in order to show the improvements associated with the windowing technique.

3.1. SOUND REDUCTION INDEX

3.1.1. *Aluminium plate*

The case of an aluminium plate, whose characteristics are given in Table 1, is first considered. First, the sound reduction index $\tau_{inf\_diffuse}$ is calculated for the infinite plate under a diffuse incident field ($0^\circ \leqslant \theta \leqslant 90^\circ$). Then, the diffuseness of the acoustic field incident in the infinite structure is reduced, as is usually done by researchers [3–5] in order to better match the computed and measured sound reduction index; the limiting angle is usually taken between 70° and 85° (instead of 90°). Finally, the spatial windowing technique

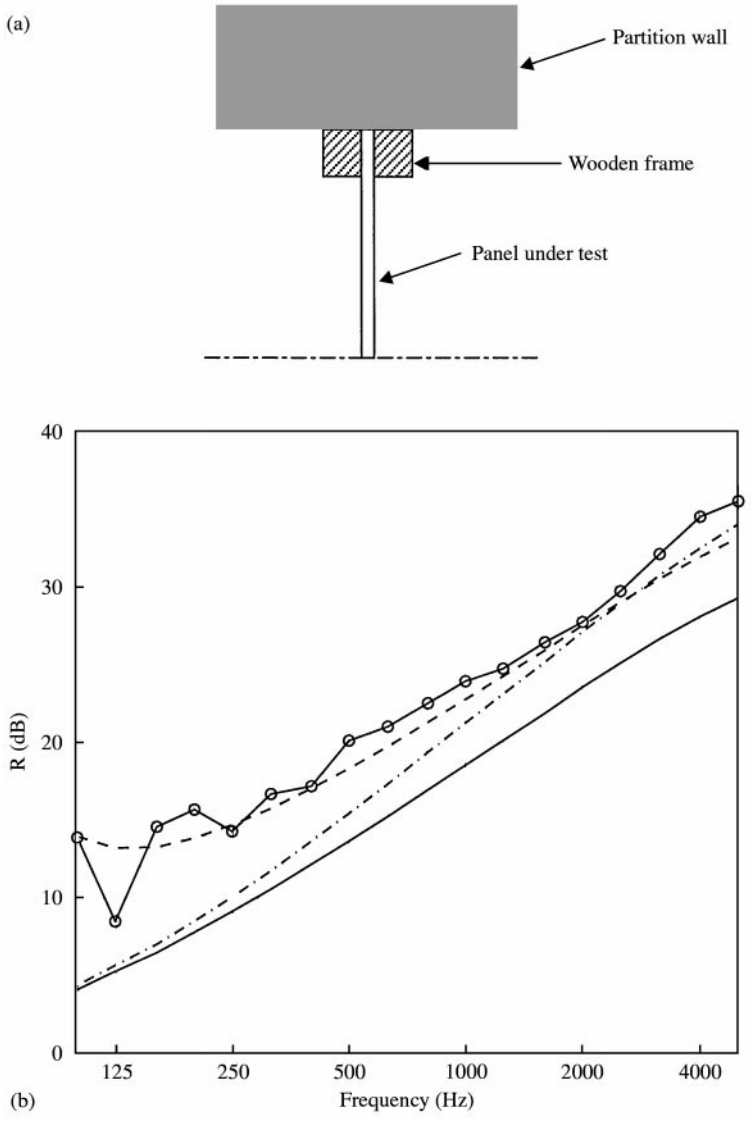

Figure 12. (a) System description and (b) Sound transmission index for an aluminum plate; ○—○ measured, — infinite system, – – – spatially windowed system, –·–· infinite system with reduced incident field diffuseness.

is applied to consider a plate of dimensions $1{\cdot}1 \times 1{\cdot}4\,\mathrm{m}^2$ and the transmission index $\tau_{finite\_diffuse}$ for a diffuse field excitation ($0^\circ \leqslant \theta \leqslant 90^\circ$) given by equations (18) and (19) is calculated. Experimental results were obtained for the panel mounted between two reverberant rooms according to Standard ISO I40-3 [14] with mounting conditions as described in Figure 12(a). Figure 12(b) shows the calculated results as well as the results measured in the laboratory in third octave bands. The sound reduction index for the infinite structure is much lower (by about 6 dB) than the measured one, but the slope of R is well represented (except at low frequencies). The result of reducing the diffuseness of incident field on the high frequency structure ($0^\circ \leqslant \theta \leqslant 78^\circ$) allows very good agreement to be achieved with the measurements in the high frequency region (above 1 kHz). However, the slope is not as good as before and the calculated results do not match the measurements in

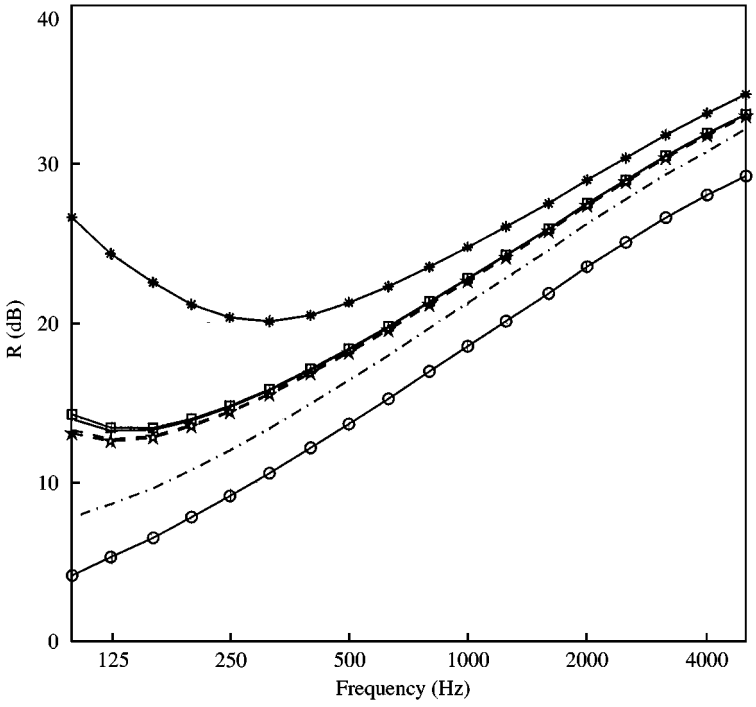

Figure 13. Sound transmission index for an aluminum plate—size effect. ○—○ infinite, ∗—∗ $0{\cdot}5 \times 0{\cdot}5\ m^2$, — $1{\cdot}4 \times 1{\cdot}1\ m^2$, □—□ $1{\cdot}2 \times 1{\cdot}2\ m^2$, – – – $1{\cdot}3 \times 1{\cdot}3\ m^2$, ☆– – –☆ $1{\cdot}5 \times 1{\cdot}2\ m^2$, · — · — · $4{\cdot}0 \times 3{\cdot}0\ m^2$.

the low frequency range. Using the spatial windowing technique developed in this paper permits a better prediction of the general behavior of the second reduction index over the entire frequency range. The small value taken by the radiation efficiency in the low-frequency range (see Figures 8 and 9) yields an important increase of the sound transmission index and allows the finite system sound transmission index (i.e., measured transmission index) to be predicted accurately. In the high frequency range (above 1·6 kHz), the spatial windowing technique and the incident field diffuseness reducing approach give very similar results. This is due to the fact that the radiation efficiency at high frequencies (see Figures 8 and 9) remains finite at angles of incidence close to 90°.

Figure 13 presents the sound reduction index for different sizes (apertures) of the aluminium plate. As expected, the smallest plate ($0{\cdot}5 \times 0{\cdot}5\ m^2$) is associated with the highest transmission index. This is due to the fact that the radiation efficiency for a small spatial window is small (smaller than unity) for any angle of incidence over an important frequency range. Increasing the size of the plate to $4{\cdot}0 \times 3{\cdot}0\ m^2$ allows the transmission index to move close to that of the infinite structure. The other sizes of the plate considered are associated to a similar surface area and therefore lead to a transmission coefficient of the same order. This shows that the windowing technique does not concentrate on the modal behavior (which would be different for all the different plate dimensions) but rather on the general behavior related to the overall dimensions of the structure.

3.1.2. *Double glazing*

The case of a double glazing is now considered. The characteristics of the glass are given in Table 1. The air space between the two identical glass panes is 12 mm thick. Figure 14

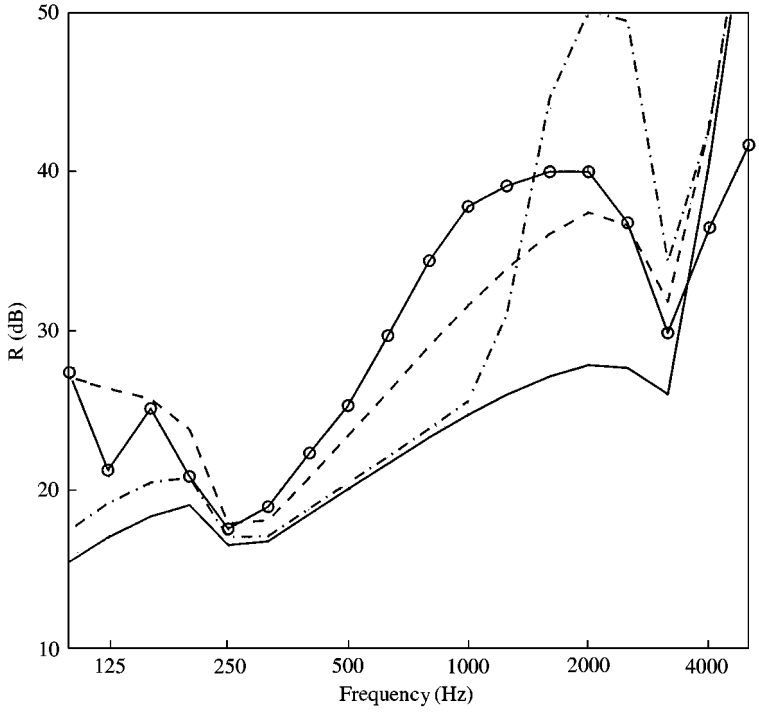

Figure 14. Sound transmission index for a double glazing; ○—○ measured, — infinite system, – – – spatially windowed system, –·–· infinite system with reduced incident field diffuseness.

shows the second reduction index for the infinite double leaf system, the results of reducing the incident field diffuseness, i.e., $0^\circ \leqslant \theta \leqslant 78^\circ$, the result for the double glazing of dimensions $1{\cdot}48 \times 1{\cdot}23$ m^2 after applying the spatial windowing technique and the measured results. The experimental results are obtained under the same conditions described for the aluminium panel in section 3.1.1. Note that the results presented in Figure 14 include damping in the air gap [15]. The model of the infinite system fails to predict a transmission index R close to the measured one; it first underestimates the transmission loss over almost the entire frequency range studied, and second it completely fails to predict the different slopes. The reduction of the incident field diffuseness is associated with quite a spectacular increase of the transmission index between 1 and 2 kHz which does not correspond to any real behavior of the system; this method is definitely not adapted to the double leaf system considered here. The use of the spatial windowing technique allows, as previously, a predicted transmission index to be much closer to the measured one: the general behavior is well represented. It should be noted that the spatial windowing affects, surprisingly, the sound transmission index in the mid-high frequency range. Indeed, this behavior is related to the fact that, in the mid-high frequency range, most of the transmitted energy is associated to the large incidence angles (the mass-air-mass resonance of the system at low frequencies in the 250 Hz third octave is mostly related to the low angles of incidence, while the critical frequency of the panes at mid-high frequencies in the 3150 Hz third octave is related to the high angles of incidence) and that the radiation efficiency at high incidence angles is modified by spatial windowing (according to the results presented in Figure 9), even for high values of k_aL (greater than 50 here).

Figure 15 presents the sound reduction index for different sizes of the double glazing. As previously mentioned, the reduction index is similar for dimensions of double glazing

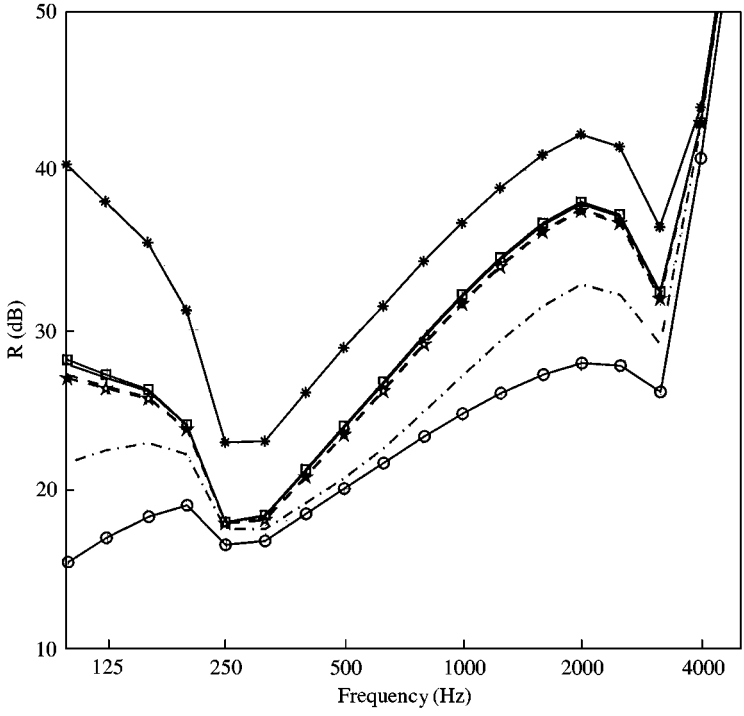

Figure 15. Sound transmission index for a double glazing—size effect. ○—○ infinite, ∗—∗ $0{\cdot}5 \times 0{\cdot}5\ m^2$, — $1{\cdot}4 \times 1{\cdot}1\ m^2$, □—□ $1{\cdot}2 \times 1{\cdot}2\ m^2$, – – – $1{\cdot}3 \times 1{\cdot}3\ m^2$, ☆– – –☆ $1{\cdot}5 \times 1{\cdot}2\ m^2$, · — · — · $4{\cdot}0 \times 3{\cdot}0\ m^2$.

associated with similar surface areas. It is also very interesting to note that the sound transmission index at the critical frequency depends strongly on the surface area considered and therefore not only on the damping coefficient of the structural components usually considered [1–3]. The sound transmission index at the mass-air-mass frequency also presents as well this type of behavior.

3.1.3. *Multi-layered panel*

The case of a multi-layered panel is now considered. The multi-layered panel consists of a 0·75 mm steel plate, 30 mm of 90 kg/m^3 mineral wool and a 3 mm laminate plate (this laminate is made of resin reinforced by celluoid fibers). The two plates are bonded (glued) to the mineral wool as well as on a wooden frame as depicted in Figure 16(a). The characteristics of the material are given in Table 2. Note that the dynamic characteristics of the laminate plate were deduced from the measurement of the input mobility on a finite beam by identifying the modal resonance frequencies. The mineral wool (porous material) is modelled following Biot's theory as described in reference [13] which includes the coupling of the solid and fluid phase of the porous material. Figure 16(b) shows the sound reduction index for the infinite panel, the result for the panel of dimensions $1{\cdot}3 \times 1{\cdot}3\ m^2$ after applying the spatial windowing technique and the measured results. The experimental results are obtained in a laboratory following the same conditions described for the aluminum panel in section 3.1.1. Once again, using the windowing technique, the small value taken by the radiation efficiency in the low frequency range yields as important increase of the sound transmission index and allows the measured transmission index to be predicted accurately.

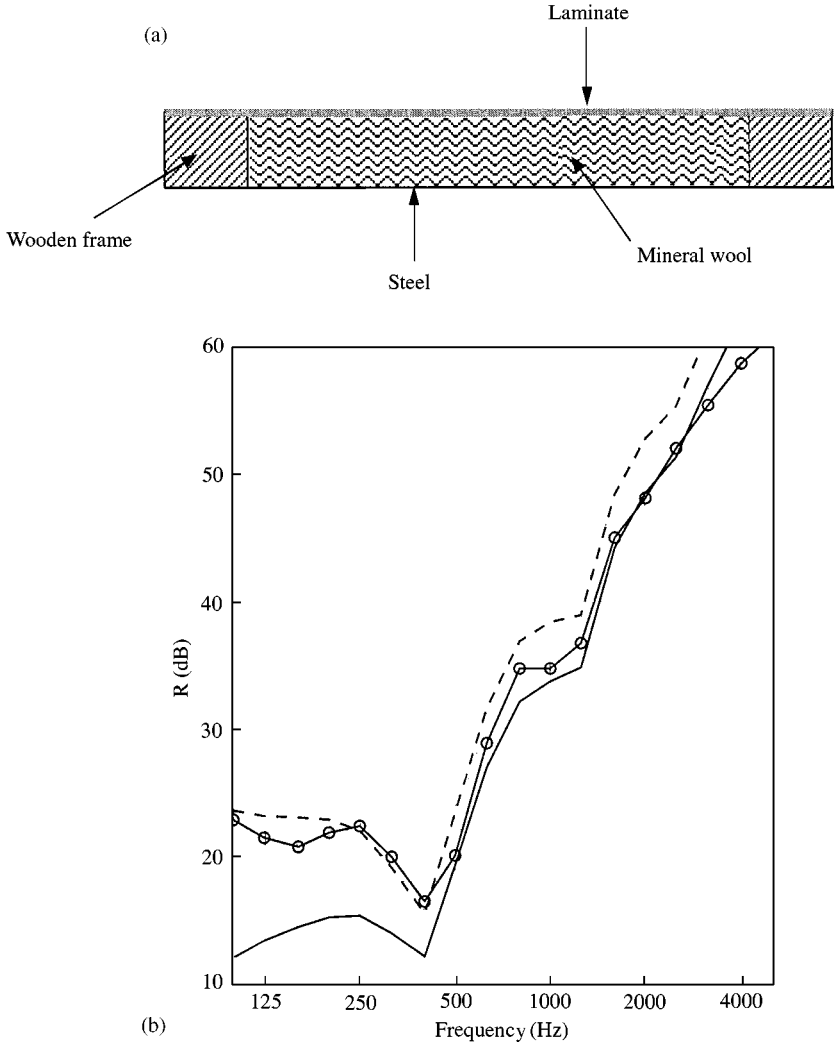

Figure 16. (a) System description and (b) Sound transmission index for a multi-layer system; O—O measured, — infinite system, – – – spatially windowed system.

3.2. MECHANICAL EXCITATION (SOUND RADIATION)

The case of a steel plate, whose characteristics are given in Table 1, is now considered. First, the sound radiation efficiency is calculated for the infinite plate under mechanical excitation (point force), then the spatial windowing technique is applied to consider a plate of length 1·3 m and width 1·2 m. Figure 17 presents in third octave bands these results as well as the experimental results. In the experimental setup, the steel plate was screwed on a heavy partition wall with a $1{\cdot}3 \times 1{\cdot}2\ \mathrm{m}^2$ aperture. The measurements were performed using Nearfield Acoustical Holography [16]; using the NAH technique, both the vibrational field of the plate and the acoustic intensity field are obtained so that the acoustic power radiated and the radiation factor can be easily calculated. Two point force positions are considered in the calculation; one at the center of the plate and one at the exact position (corresponding to force position during the measurements, i.e., at 0·4 m from the length edge

TABLE 2

Multi-layered characteristics

	Steel	Mineral wool	Laminate
Thickness	0·75 mm	30 mm	3 mm
Young's modulus	210. GN/m^2	0·4 MN/m^2	0·6 GN/m^2
Density	7850 kg/m^3	90 kg/m^3	1360 kg/m^3
The Poisson ratio	0·3	0	0·15
Damping	3%	18%	15%
Flow resistivity		34 kNs/m^4	
Tortuosity		1	
Porosity		0·955	
Characteristic dimension Λ		40 μm	
Characteristic dimension Λ'		80 μm	

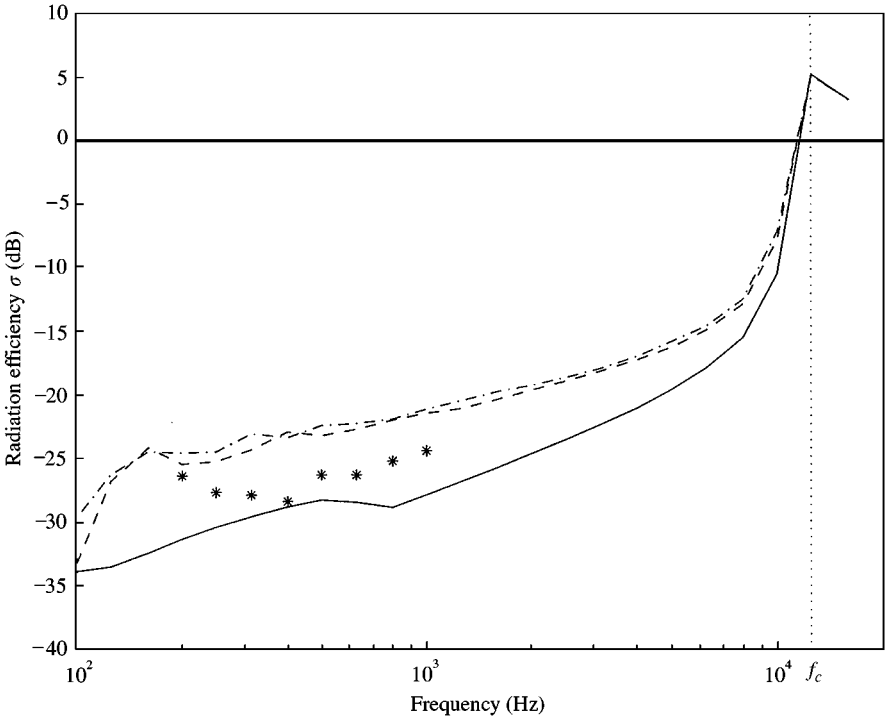

Figure 17. Sound radiation efficiency for a steel plate. ∗ measured, — infinite system, – – – spatially windowed system with force centered, –·–· spatially windowed system with exact force position.

and 0·3 m from the width edge). In this case, the force location has little impact on the calculated radiation efficiency. The measured radiation efficiency is between the radiation efficiency obtained with spatial windowing and that calculated without spatial windowing.

Figure 18 presents the sound radiated power calculated using equation (23) and corresponding to the different cases considered in Figure 17. The force level during the measurement was recorded and used to normalize the measured radiated power to an excitation force of 1 N. It can be seen that the radiated power using the spatial windowing technique is very close to the measured radiated power. In this case, the radiated power is

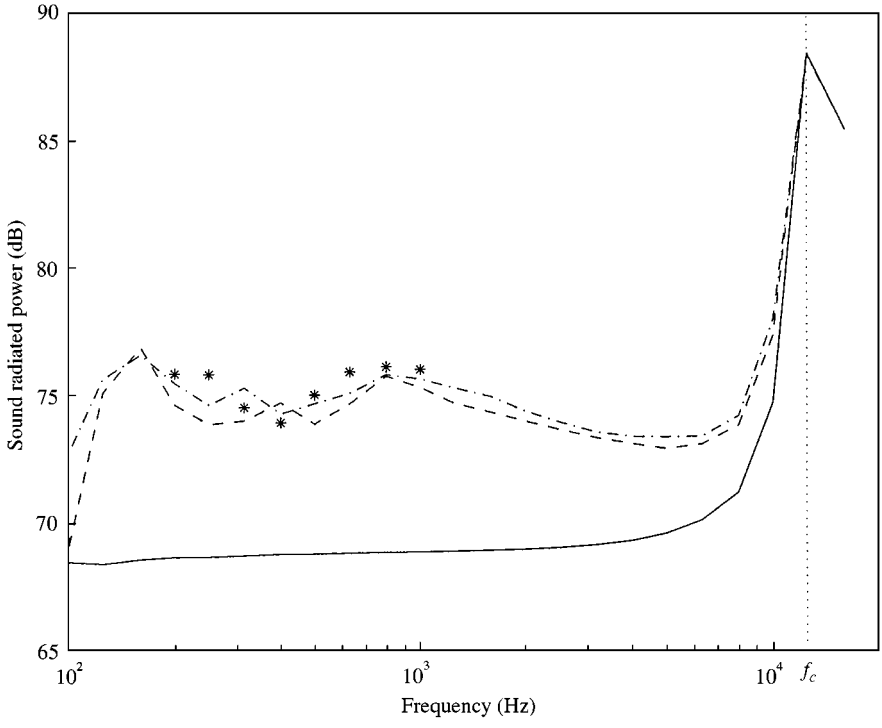

Figure 18. Sound radiated power for a steel plate; ∗ measured, — infinite system, – – – spatially windowed system with force centered, – · – · spatially windowed system with exact force position.

predicted within 2 dB. The predicted radiated power using the exact force location provides slightly better results (closer to the experimental data) than those using the force at the center of the plate.

Figure 19 presents the calculated radiation efficiency of the steel plate considered for different aperture sizes. The excitation force is assumed to be at the center of the plate. As previously mentioned, the radiation efficiency is similar for dimensions of the plate associated to similar surface areas. As the size of the plate increases to $4{\cdot}0 \times 3{\cdot}0\ \mathrm{m}^2$, the radiation efficiency of the spatially windowed system approaches that of the infinite structure. As mentioned previously (see section 2·4 and Figure 10), the important decrease in the radiation efficiency observed at 160 Hz third octave for a system size of $0{\cdot}5 \times 0{\cdot}5\ \mathrm{m}^2$ occurs when the flexural wavelength is half of the system characteristic dimension ($L = 0{\cdot}5$ m). Note that for the other sizes considered here, this phenomenon takes place below or close to the 100 Hz third octave.

4. CONCLUSIONS

A technique based on a spatial windowing has been presented in order to take the finite size of a plane multi-layered structure into account. It relies on the wave approach, therefore allowing advantage to be taken of the relative simplicity of transfer matrix approach for infinite multi-layered structures (without any modal consideration) and introduces the diffraction effect associated with the finite size of a structure using spatial windowing. In the case of sound transmission, the technique is very simple and the calculation of the radiation efficiency depends only on the spatial window considered; this incidence dependent

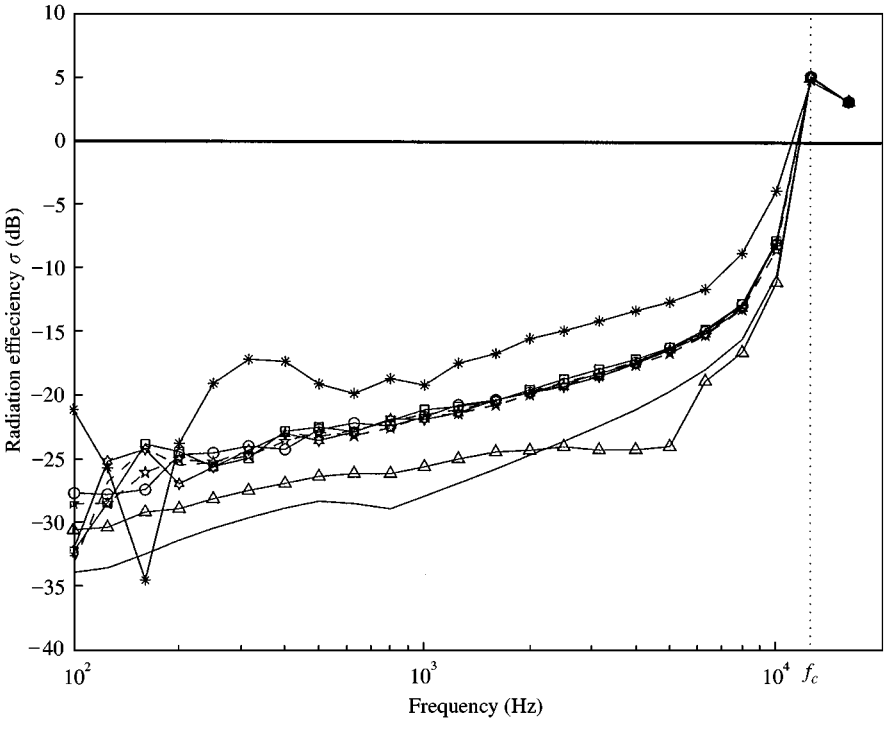

Figure 19. Sound radiation efficiency for a steel plate—size effect; — infinite, ∗—∗ $0{\cdot}5 \times 0{\cdot}5\ m^2$, ○—○ $1{\cdot}4 \times 1{\cdot}1\ m^2$, □—□ $1{\cdot}2 \times 1{\cdot}2\ m^2$, – – – $1{\cdot}3 \times 1{\cdot}2\ m^2$, ★—★ $1{\cdot}3 \times 1{\cdot}3\ m^2$, ☆– – –☆ $1{\cdot}5 \times 1{\cdot}2\ m^2$, △—△ $4{\cdot}0 \times 3{\cdot}0\ m^2$.

radiation efficiency can therefore be pre-calculated. In the case of mechanical excitation, the technique is more complicated, as the radiation efficiency depends on the vibration behavior of the plate considered and involves either the calculation of a two-dimensional convolution product or a two-dimensional inverse Fourier transform. Nevertheless, these can be calculated in a reasonable time with current computers. Predicted results including the sound transmission index of an aluminum plate, a double glazing panel and a multi-layer panel, as well as the radiation efficiency and the radiated power of a mechanically excited metal plate, were presented and compared with experimental results in order to validate the technique. With spatial windowing, calculated results in terms of sound transmission, radiation efficiency and radiated sound power were surprisingly very close to measured results, showing that the finite aperture effect is very important in sound radiation and sound transmission. This technique appears to provide a good trade-off between computation cost and modelling accuracy.

REFERENCES

1. F. FAHY 1995 *Sound and Structural Vibration, Radiation, Transmission and Response*. London: Academic Press.
2. M. L. MUNJAL 1993 *Journal of Sound and Vibration*, **162**, 333–343. Response of a multi-layered infinite plate to an oblique plane wave by means of transfer matrices.
3. K. A. MULHOLLAND, H. D. PARBROOK and A. CUMMINGS 1967 *Journal of Sound and Vibration*, **6**, 324–334. The transmission loss of double panels.
4. J. S. BOLTON, N.-M. SHIAU and Y. K. KANG 1996 *Journal of Sound and Vibration*, **191**, 317–347. Sound transmission through multi-panel structures lined with elastic porous materials.

5. B. BROUARD, D. LAFARGE and J.-F. ALLARD 1995 *Journal of Sound and Vibration*, **183**, 129–142. A general method of modeling sound propagation in layered media.
6. H. SATO 1973 *Journal of the Acoustical Society of Japan*, **29**, 509–516. Transmission of traffic noise through windows—Influence of incident angle on sound insulation in theory and experiments.
7. J. H. RINDEL 1975 *The Acoustics Laboratory*, *Technical University of Denmark*, Report no. 9. On the mechanism of outdoor noise transmission through walls and windows.
8. S. LJUNGGREN 1991 *Journal of the Acoustical Society of America*, **89**, 2324–2337. Airborne sound insulation of thin walls.
9. E. C. SEWELL 1970 *Journal of Sound and Vibration*, **12**, 21–32. Transmission of reverberant sound through a single-leaf partition surrounded by an infinite rigid baffle.
10. F. G. LEPPINGTON, E. G. BROADBENT, F.R.S., K. H. HERON and S. M. MEAD 1986 *Proceedings of the Royal Society of London*, A **406**, 139–171. Resonant and non-resonant acoustic properties of elastic panels. I. The radiation problem.
11. F. G. LEPPINGTON, K. H. HERON, E. G. BROADBENT, F.R.S., and S. M. MEAD 1986 *Proceedings of the Royal Society of London*, A **412**, 309–337. Resonant and non-resonant acoustic properties of elastic panels. II. The transmission problem.
12. C. LESUEUR 1988 *Rayonnement acoustique des structures.* Paris: Academic Press.
13. J. F. ALLARD 1993 *Propagation of Sound in Porous Media—Modelling Sound Absorbing Materials.* London: Elsevier Science Publishers.
14. Standard ISO 140-3 1995 *Second Edition. Acoustics—Measurement of sound insulation in buildings and of building elements—Part 3: Laboratory measurements of airborne sound insulation of building elements.*
15. L. GAGLIARDINI April 1991 *Ph.D. Thesis*, *Institut National des Sciences Appliquées de Lyon*, Lyon. Simulation numérique de la transmission acoustique par les parois simples et multiples.
16. M. VILLOT, G. CHAVÉRIAT and J. ROLAND 1992 *Journal of the Acoustical Society of America*, **91**, 187–195. Phonoscopy: An acoustical holography technique for plane structures radiating in enclosed spaces.